Neuron Glia Biology, 2007, 3, 335–351. ©2008 Cambridge University Press
doi:10.1017/S1740925X08000185 Printed in the United Kingdom

Reactive astrocytosis and glial glutamate transporter clustering are early changes in a spinocerebellar ataxia type 1 transgenic mouse model

ROBERTO GIOVANNONI[1]
NICOLA MAGGIO[2]
MARIA ROSARIA BIANCO[2]
CARLO CAVALIERE[2]
GIOVANNI CIRILLO[2]
MARIALUISA LAVITRANO[1,3]
AND
MICHELE PAPA[2,3]

Spinocerebellar ataxia type 1 (SCA1) is a neurodegenerative disorder caused by an expanded CAG trinucleotide repeats within the coding sequence of the ataxin-1 protein. In the present study, we used a conditional transgenic mouse model of SCA1 to investigate very early molecular and morphological changes related to the behavioral phenotype. In mice with neural deficits detected by rotarod performance, and simultaneous spatial impairments in exploratory activity and uncoordinated gait, we observed both significant altered expression and patchy distribution of excitatory amino acids transporter 1. The molecular changes observed in astroglial compartments correlate with changes in synapse morphology; synapses have a dramatic reduction of the synaptic area external to the postsynaptic density. By contrast, Purkinje cells demonstrate preserved structure. In addition, severe reactive astrocytosis matches changes in the glial glutamate transporter and synapse morphology. We propose these morpho-molecular changes are the cause of altered synaptic transmission, which, in turn, determines the onset of the neurological symptoms by altering the synaptic transmission in the cerebellar cortex of transgenic animals. This model might be suitable for testing drugs that target activated glial cells in order to reduce CNS inflammation.

Keywords: EAAT1, synaptic plasticity, SCA1, neurodegeneration

INTRODUCTION

The contribution of non-neuronal cells to the pathogenesis of neurodegenerative diseases has been described although the mechanism remains poorly understood. The role of neuron–glia interactions is also being investigated in neurodegenerative diseases such as amyotrophic lateral sclerosis (ALS) and Alzheimer's disease (Sheldon and Robinson, 2007). Moreover, glial dysfunction is likely to contribute to the pathogenesis of cerebellar ataxia in a mouse model of spinocerebellar ataxia type 7 (SCA7) (Custer *et al.*, 2006).

Excitatory amino acids transporter 1 (EAAT1, also known as GLAST) is the major glutamate transporter in the cerebellum (Lehre and Danbolt, 1998). It is expressed strongly by astrocytes in the molecular layer of the cerebellum and is at highest density on Bergmann glia. EAAT1 is not detected in neurons (Ginsberg *et al.*, 1995). EAAT1 present on the plasma membrane of the astrocytic processes and cell bodies (Chaudhry *et al.*, 1995). Targeting of EAAT1 is regulated carefully on astroglial membranes facing the neuropil, large dendrites, cell bodies and capillary endothelium (Danbolt, 2001). Therefore, its distribution follows the morphological changes of astrocytes during inflammatory processes. Recently, in a mouse model of reactive astrocytosis in the spinal cord, it has been reported that this glial process includes a marked proteolytic cascade having as substrates glial transporters. Subsequent changes in neurotransmitter uptake represent the basis of morphological and functional changes that sustain central plasticity (Cavaliere *et al.*, 2008). Moreover, glial activation involves changes in cell phenotype and gene expression that might trigger glial-induced neuronal death (Bal-Price and Brown, 2001). Glial-mediated inflammatory responses appear to have a key role in the pathophysiology of several neurodegenerative disorders that involve early activation of microglia and astrocytes (Mrak and Griffin, 2005). In general, overexpression of cytokines appears several years before pathological changes are evident (Griffin *et al.*, 2006). The time needed for glial activation might explain the mid-life onset of many neurodegenerative disorders, even those that are genetically determined, before the patient displays the full clinical symptoms of the disease (Unger, 1998).

Spinocerebellar ataxia type 1 (SCA1) is a dominantly inherited, progressive, neurological disorder, that is char-

acterized clinically by ataxia and cranial motor neuropathies in the absence of cognitive deficits. SCA1 belongs to the polyglutamine disorders, a group of inherited neurodegenerative diseases caused by expansion of a translated CAG repeat in the coding region of the *SCA1* gene (Schols *et al.*, 2004; Orr and Zoghbi, 2007). The characterization of *SCA1* (Banfi *et al.*, 1994) allowed ataxin-1 (ATAXIN1) the protein it encodes, to be identified as the molecule responsible for disease pathogenesis and progression. ATAXIN1 is expressed in the CNS throughout life, localized mainly in the nucleus, both in its normal and mutated configuration, with some cytoplasmic localization in cerebellar Purkinje cells (Servadio *et al.*, 1995). Characteristic neuropathological findings in SCA1 are the loss of Purkinje cells in the cerebellum and neurons in the inferior olivary complex (Robitaille *et al.*, 1995). As described for other polyglutamine diseases such as Huntingdon's disease (HD) (DiFiglia *et al.*, 1997; Davies *et al.*, 1997), the presence of neuronal intranuclear inclusions (NIs) in Purkinje cells in human patients (Servadio *et al.*, 1995) and in a transgenic mouse model (Skinner *et al.*, 1997) represents a pathological hallmark of SCA 1. Recent evidence shows that compounds that increase inclusion formation might reduce cellular pathology in several neurodegenerative disorders (Bodner *et al.*, 2006).

Several animal models have been generated and investigated (Burright *et al.*, 1995; Fernandez-Funez *et al.*, 2000; Watase *et al.*, 2002; Emamian *et al.*, 2003; Chen *et al.*, 2003) in order to understand the processes that underlie the onset and progression of SCA1. Data show that mutant ATAXIN1 protein levels have a key role in modulating disease pathogenesis. The expanded tracts are relatively resistant to proteasomal degradation (Paulson, 1999), which leads to the accumulation of polyglutamine-containing peptide fragments within the cell. To define the role of different protein domains in the onset and progression of the disease, models that differ in either the length of the polyQ tract inserted (Lorenzetti *et al.*, 2000) or the specific mutation induced (Klement *et al.*, 1998) have been generated. To investigate the cellular pathways that influence disease progression, SCA1 transgenic mice have been crossed with either transgenic mice or mice that are deficient in genes involved specifically in protein degradation or stress responses (Cummings *et al.*, 1999; Shahbazian *et al.*, 2001; Cummings *et al.*, 2001; Okuda *et al.*, 2003). Recently, it has been demonstrated that blocking the expression of mutant ATAXIN1 in a conditional mouse model of SCA1 modifies the progression of the disease (Zu *et al.*, 2004; Serra *et al.*, 2006). The majority of these models are somewhat limited because they involve the expression of the polyQ tract mainly in cerebellar Purkinje cells. In humans, *SCA1* is expressed throughout the brain, including non-neuronal cells. In a HD mouse model expressing 77 CAG repeats, glial fibrillary acidic protein (GFAP)-positive cells increase in the brains without any signs of neuronal degeneration (Ishiguro *et al.*, 2001) and in genetically modified models of SCA7 it has been demonstrated that dysfunction of Bergmann glia leads to non-cell autonomous Purkinje cell degeneration in the absence of expression of mutant ataxin-7 in Purkinje cells. Moreover, GLAST-deficient mice fail motor challenging tasks and GLAST has active roles in synapse formation of cerebellar climbing fibre and in preventing excitotoxic cerebellar damage (Watase *et al.*, 1998).

OBJECTIVE

To identify and better clarify each step in the pathogenesis of SCA1 we generated a conditional mouse model using the tetracycline-responsive gene (TET) system to control the expression of ATAXIN1 containing different polyQ repeats (either 32Q or 100Q). To fully reproduce the molecular and genetic features of this devastating condition we used a brain-specific promoter to induce ATXIN1 throughout brain tissues, as occurs in humans. We have used this model to analyze the modifications that affect the neuro-glial network (mainly the tripartite synapse) to clarify the early alterations that lead to death of Purkinje cells at advanced stages.

METHODS

Transgenic constructs

Two different responder constructs have been generated. cDNAs encoding normal and expanded ATAXIN1 (32 and 100 CAG repeats, respectively; TRE-nSCA and TRE-eSCA constructs) with a short 5′UTR region from the *SCA1* gene, were subcloned independently downstream of the TET-responsive element (TRE) promoter in the pUHD10–3 plasmid (Gossen and Bujard, 1992). In both constructs a c-myc tag sequence was fused in-frame to the coding region. These two constructs have been used successfully *in vitro* (Rimoldi *et al.*, 2001).

Production and maintenance of TET transgenic mice

Following removal of the vector backbone by digestion with Ssp I and Nsp I, the TRE-nSCA (3.7 Kb) and the TRE-eSCA (3.9 Kb) constructs were microinjected independently into oocyte pronuclei from C57BL/6J × DBA2 F1 hybrids (BDF1). Founder mice were identified by PCR and Southern blot analyses. Nine of the 11 TRE-nSCA and 14 out of 19 TRE-eSCA founder mice bred successfully, originating transgenic lines. Responder Tg mice analyzed in this study were hemizygous for the transgene. A few transgenic strains were then transferred to a FVB/N inbred genetic background. To induce expression of human ATAXIN1 in the brains of transgenic mice, the PrP-tTA (F959 line) (Tremblay *et al.*, 1998) transgenic line was used, which expresses tTA at high levels in all brain regions (Boy *et al.*, 2006).

Doxycycline treatment

Doxycycline (Dox) treatment was performed as follows: PrP-tTA and TRE-SCA transgenic females were given 0.5 mg ml^{-1} Dox in 5% sucrose solution instead of the normal drinking water for 7 days before mating. Dox was then either withdrawn [ATAXIN1 expression in young, double transgenic mice (DTg)] or continued (constitutive repression of ATAXIN1 expression). Dox solution was maintained in dark bottles and changed three times a week.

Genotype analysis

Genotyping analyses were performed using DNA extracted from mouse tail biopsies. SCA1 responder Tg mice: specific

primers that anneal to the TRE promoter (oligo forward: 5′-ACCCGGGTCGAGTAGGCG-3′) and after the CAG repeat sequence (oligo reverse: 5′-GCTCTTCTCCATCTCACCGT-3′) were used, resulting in fragments of either 1228 bp (32 CAG Repeats) or 1432 bp (100 CAG Repeats). Southern blot analyses used the TRE sequence as probe.

TET activator Tg mice: Specific primers (oligo forward: 5′-AAGTAAAGTGATTAACAGCGC-3′; oligo reverse: 5′-CTACCCACCGTACTCGTC-3′) were used, resulting in a 1042 bp amplification fragment.

RT-PCR analyses

Total RNA was extracted from half of the cerebellum or brain using Trizol reagent (Invitrogen), following the manufacturer's recommended protocol. cDNA was prepared from either 1 μg (TRE-SCA transgene products) or 40 ng (GFAP and EAAT1 endogenous genes) of total RNA with oligo dT primers (Promega) using SuperScript III reverse transcriptase (Invitrogen), following the manufacturer's recommended protocol. The cDNA (1/10 of the final volume) was amplified by PCR as follows: 1 cycle of 9 min at 94°C; 25–33 cycles of 30 sec at 94°C, 30 sec at a primer pair-specific temperature and 30 sec at 72°C; 1 cycle of 10 min at 72°C. Primers were designed for each endogenous gene using Primer3 software (Rozen and Skaletsky, 2000): GFAP, forward 5′-AGAAAACCGCATCACCATTC-3′, reverse 5′-TCACAT-CACCACGTCCTTGT-3′; EAAT1, forward 5′-CCAAAAGC-AACGGAGAAGAG-3′, reverse 5′-ACCTCCCGGTAG-CTCATTTT-3′; β-actin, forward 5′-GTGGGCCGCCC-TAGGCACCAG-3′, oligo 5′-GAAATCGTGCGTGACATC-AAAGAG-3′. The linear range of PCR amplification for each primer pair was determined. In all PCR reactions β-actin gene was used as the endogenous control. Amplification products were run on 1.5–2% agarose Tris acetate EDTA gel, stained with ethidium bromide and gel images captured with GelDoc System (Bio-Rad Laboratories). Bands were quantified using Quantity One software (Bio-Rad Laboratories). Genomic DNA contamination was checked.

Immunoblot analyses

Tissues were homogenized in 50 mM Hepes pH 7.5, 10% glycerol, 10 mM NaCl, 10 mM dithiothreitol, 1% SDS, 5 mM EDTA and protease inhibitors (Sigma Aldrich). Protein extracts (10 μg) were run on a 10% Tris-glycine gel and transferred to nitrocellulose (Amersham Biosciences). After blocking non-specific sites (5% milk in TBST, 20 mM Tris-HCl, pH 7.4, 100 mM NaCl, 0.2% Tween 20), membranes were incubated with either anti-ATAXIN1 11NQ (Servadio *et al.*, 1995) or anti-β-actin (Table 1) for 2 hours at room temperature, washed in TBST, and incubated with peroxidase-conjugated (anti-rabbit for 11NQ or anti-mouse for anti-β-actin) secondary Ab (1:5000; Amersham Biosciences) for 1 hour. Immunoreactivity was detected with enhanced chemiluminescence (Amersham Biosciences).

Animals

Mice were housed four–five per cage with food and water available *ad libitum* and maintained in a temperature- and humidity-controlled environment on a 12-hour light/dark cycle. Experiments were carried out according to a protocol approved by the animal care committee of the Minister of Public Health, and in accordance with guidelines from the European Union and NIH guide for care and use of laboratory animals. In all experiments, control mice were

Table 1. Antibodies used for immunohistochemistry

Antiserum	*Immunogen*	Source/cat. no.	Dilution	Antigen	Reference
Guinea pig anti-glutamate transporter (EAAT1)	Synthetic peptide from carboxy-terminus of rat EAAT1	Chemicon International # AB 1782	1:4000	Glutamate transporters expressed in glial cells	(Suarez, 2000)
Mouse anti-glial fibrillary acidic protein (GFAP)	Purified GFAP from pig spinal cord	Sigma # G3893	1:400	Specific intermediate filaments protein in astrocytes	(Franke, 1991)
Mouse anti c-myc	A synthetic peptide corresponding to residues 408–439 of the human p-62$^{c\text{-}myc}$, protein conjugated to KLH	Sigma # M4439	1:400	Epitope located within the sequence EQKLISEEL (residues 410–419) of the product of the human oncogene c-myc, known as the c-myc tag	(Campbell, 1992)
Mouse anti-calbindin-D-28K (Cb28K)	Purified bovine kidney calbindin-D-28K	Sigma # C9848	1:15 000	Cb28K (28 kDA)	(Chard, 1995)
Rabbit anti-Cb28K	Recombinant rat calbindin D-28k	Swant # CB-38a	1:10 000	Cb28K	(Oh *et al.*, 2007)
Mouse anti-β actin	A slightly modified synthetic β-cytoplasmatic actin N-terminal peptide Ac-Asp-Asp-Asp-Ile-Ala-Leu-Val-Ile-Asp-Asn-Gly-Ser-Gly-lys conjugated to KLH.	Sigma # A5441	1:5000	Epitope located on the N-terminal end of the β-isoform of actin	(North, 1993)
Rabbit anti-ATAXIN1 (11NQ)	N-terminal peptide (amino acids 164–197) of ATAXIN1 conjugated through its N-terminus to keyhole limpet haemocyanin	Kind donation from Drs Servadio and Zoghbi	1:6000	Epitope located on the N-terminal peptide of ATAXIN1	(Skinner, 1997)

wild-type mice and single transgenic, expressing only the activator tTA protein or carrying the responder transgene, because these did not show any difference in all the behavioral and morphological analyses performed.

Behavioral analysis

Neurological alterations were detected until 20 weeks after the birth. To characterize the early alterations in rearrangement of the neuro–glial network we analyzed 11-week-old DTg mice when the phenotype alterations become stable.

Open-field test

This test was performed to assess exploratory behavior and general locomotor activity. We analyzed DTg and control mice. Mice were placed into the center of a 70 × 100 cm open arena containing a 10 × 10 cm gridded floor, for 15 min per test for six consecutive days (Clark *et al.*, 1997). On the fourth day of testing, an enriched open-field test was performed by placing three different objects in the arena. These objects remained in the same position on the fifth day, but we changed their location on the sixth day. Activities of animals were videotaped for 15 min. Each trial was divided into 5-min intervals so that the total number of grid crossings and the latency to reach the periphery of the arena, after the animal was introduced, could be analyzed. Data were analyzed by one-way ANOVA, followed by *post hoc* Bonferroni's multiple comparison tests; $P<0.0001$ was considered statistically significant (StatView; Abacus Concepts).

Accelerating rotarod test

We used the rotarod test to assess the ability of mice to improve their motor skill performance by training. This study was performed on naïve animals only. Mice were placed on the rotarod apparatus (Ugo Basile) for four trials per day for 4 consecutive days (Clark *et al.*, 1997). Each trial lasted a maximum of 10 min, divided into an initial part in which the rotarod underwent a linear acceleration from 4–40 rpm over the first 5 min of the trial and then remained at maximum speed for the remaining 5 min. Animals were scored for their latency to fall and for the number and time spent in holding for each trial. Data were analyzed by one-way ANOVA, followed by *post hoc* Bonferroni's multiple comparison tests; $P<0.0001$ was considered statistically significant (StatView).

Footprint analysis

After coating the hind feet of the mice with a non-toxic paint, animals were allowed to walk through a dark, 40-cm long, 9-cm wide, 6-cm high tunnel, and the footprint patterns made on the paper lining the floor of the tunnel were scored for four step parameters (Clark *et al.*, 1997). Step length: the average distance of forward movement between alternate steps. Gait width: the average lateral distance between opposite left and right steps. Alternation coefficient: the value describing the uniformity of step alternation. Linear movement: the average change in angle between consecutive right-right steps. A large linear movement measurement indicates non-linear movement, or weaving, through the tunnel. Statistical significance was calculated by Student's *t*-test.

Cerebellar injury

The experiments were performed on five male FVB mice at the age of 2.5–3 months. The surgery was performed under chlorydrate tiletamine (Zoletyl) (40 mg kg^{-1}) anesthesia. Animals were mounted in a stereotaxic apparatus. After opening the skin, a sterile disposable needle (21G) was inserted into the paravermal cerebellar cortex through a burr hole of the skull (Ajtai and Kalman, 1998). The volume of the cone-like injury was ~0.08 mm^3, bleeding stopped within several seconds and the rate of respiratory movements quickly normalized spontaneously.

After surgery and suturing muscles and skin over the wound, each of the five animals was kept with great care, including prevention of infection and free access to food and water during a 12-hour light/dark cycle. At 4 days post-surgery the animals showed motor deficits resulting from cerebellar impairment. On the same day the mice were sacrificed and the brains processed.

Histological examination and immunocytochemistry

DTg and control mice were anesthetized deeply with an intraperitoneal injection (300 mg kg^{-1} body weight) of chloral hydrate and perfused transcardially with standard Ringers solution followed by 4% paraformaldehyde in 0.01 M phosphate-buffered saline (PBS), pH 7.4 at 4°C. The brains were removed and post-fixed for 2 hours in the same fixative, soaked in 30% sucrose PBS and frozen in chilled isopentane on dry ice. Immunocytochemical staining was performed on serial sections, as reported previously (Papa *et al.*, 2003), using both polyclonal and monoclonal antibodies. Free-floating sections were preincubated in PBS containing 10% normal serum and 0.25% Triton X-100 for 1 hour at 4°C and then incubated in either rabbit anti-ATAXIN1 antiserum 11NQ (Table 1) or guinea pig anti-glutamate transporter EAAT1 (Table 1) for 48 hours. For monoclonal antibody staining, sections were incubated in a mouse Ig-blocking reagent, then preincubated in a 'Protein Concentrate' solution (MOM kit, Vector Labs). Sections were incubated in either mouse anti-GFAP monoclonal antibody (Table 1), mouse anti-calbindin D-28k (CbD28k) monoclonal antibody (Table 1), or mouse anti-c-myc monoclonal antibody (Table 1). Sections were incubated with the appropriate biotinylated secondary antibody (Vector Labs; 1:200). Sections for both monoclonal and polyclonal immunostaining were processed using the Vectastain avidin-biotin peroxidase kit (ABC), (Vector Labs), and reacted with 3,3′-diaminobenzidine tetrahydrochloride (DAB; 0.5 mg ml^{-1} Tris-HCl; Sigma) and 0.01% hydrogen peroxide. Sections were mounted on chrome-alume gelatin coated slides and cover slipped. Adjacent sections were Nissl-stained. DAB-stained sections were imaged with a Zeiss Axioskope 2 light microscope (Zeiss) equipped with high-resolution digital camera (C4742–95, Hamamatsu Photonics). Double staining was performed as reported (Papa *et al.*, 2003). Sections were incubated with anti-ATAXIN1 (11NQ) and anti-CbD28k, anti-ATAXIN1 (11NQ) and anti-c-myc, or anti-calbindin D28k and

anti-EAAT1. To analyze the spatial neuro–glial arrangement, triple staining was performed in which sections were incubated with anti-calbindin D28k, anti-GFAP and anti-EAAT1. 2-hour incubations with a cocktail of Alexa fluor 488 antirabbit IgG (1:200) and Alexa Fluor 546 antimouse IgG (1:200; Molecular Probes) was used for double staining, and an Alexa Fluor 647 antiguinea pig IgG (1:200) added for triple staining. Sections were mounted and cover-slipped with Vectashield (Vector Labs) and imaged with a laser-scanning confocal microscope (Meta-LSM 510; Zeiss). Confocal images were acquired from the cerebellar cortex region using 20 × and oil-immersion 40 × objective lenses (Zeiss). Appropriate controls lacking primary antibodies were performed for each antibody. For double immunostaining, slices were processed completely through the first series of reactions, rinsed and followed by the second series of immunoreactions. Images were captured at a resolution of 512 × 512 pixels. The appropriate argon laser fluorescence for visualization of the Alexa Fluor 488 was used with an excitation wavelength of 488 nm and emission filter BP 505–530. The HeNe laser fluorescence for the visualization of Alexa Fluor 546, with an excitation wavelength of 543 nm and emission filter LP 560. For triple localization the emission filter BP 560–615 for Alexa Fluor 546, and the HeNe laser fluorescence for the visualization of Alexa Fluor 647, with an excitation wavelength of 633 nm, and emission filter LP 638 was used. A series ($n = 57$) of single sections were acquired at 0.54 μm apart.

Cytology of Purkinje cells and analysis of spine density

Purkinje cells from 11- and 20-week-old DTg mice were recognized by Calbindin staining conjugated with the fluorescent dye Alexa-546 (absorption at 556 nm, emission at 573 nm; Molecular Probes). Fluorescent slices were imaged using a laser-scanning confocal microscope (Meta-LSM 510; Zeiss) with a 63 × oil-immersion lens. Optical z-sections were acquired at 0.5-μm steps through the apical dendritic tree of Purkinje cells. Dendritic projections of length 1–3 μm were identified as spines and counted off-line using computer assisted image analysis system (MCID 7.0; Imaging Res. Inc.); care was taken to ensure that each spine was counted only once by following its course through the optical z-section reconstruction. Purkinje cell dendrites were divided into a proximal category of dendrites (with a diameter $\geqslant$1.5 μm) and a distal category (with a diameter $<$1.5 μm). Spine density was calculated by dividing the total number of spines per dendrite by the length of the dendrite (Papa *et al.*, 1995; Tyler *et al.*, 2006). Statistical significance was calculated by Student's *t*-test.

Electron microscopy

Mice were perfused transcardially with saline followed by 2.5% glutaraldehyde, 2% paraformaldehyde, 1 mM $CaCl_2$ and 2 mM $MgCl_2$ at pH 7.4, 40–45°C. The brains were removed and post-fixed in 2% paraformaldehyde overnight at 4°C. Vibratome sections (70 μm thick) were osmicated in 2% OsO_4 in PB for 20 min, small parts were dissected from the vermian, paravermian and hemispheric cerebellum, and dehydrated through increasing gradients of ethanol, followed by acetone and embedded in Araldite. Ultrathin sections (90 nm) were lightly counterstained with 5% aqueous uranyl acetate and examined with a Zeiss EFTEM Lybra 120 electron microscope (Zeiss).

Measurements and statistical analysis

Light microscopy

The analysis of the markers and electron micrographs, was accomplished by a computer assisted image analysis system (MCID 7.0; Imaging Res. Inc.). The image analysis at light microscope was performed as reported previously (Saulle *et al.*, 2004). Briefly, to analyze the activated glia we measured the area labeled by GFAP expression as the proportional area within the molecular layer of the cerebellum; this value express the total target area relative to the scanned area. The averages were obtained from six, randomly selected cerebellar sections for each animal, and comparisons made between DTg and control groups. In the same region, to analyze the expression of EAAT1 we measured the mean density (Density-ROD); ROD is an inverse logarithmic function of gray-level values. To evaluate the distribution of the EAAT1 in the cerebellar molecular layer of DTg and controls, we calculated the ratio between the mean density value of all the pixels in the area (IOD-levels) and the standard deviation of the value (IOD/SD).

Electron microscopy

For electron microscopy analysis, we chose a previously reported systematic sampling method to reduce sampling bias (French and Totterdell, 2004). This was achieved by collecting five sections per grid on three grids, then 4 μm of the block was removed and the collection repeated, this procedure was repeated eight times. This technique allows sampling throughout the depth of the sample. The middle section of the middle grid in each collection of three grids was photographed. As an alternative, on one section we acquired four pictures proceeding from the top left corner to the bottom right corner; on the following section, we inverted direction of acquisition from the top right corner to the bottom left one.

In each electron micrograph, all asymmetric synapses (Peters *et al.*, 1991) were analyzed. Synaptic complexes were defined as structures that met two criteria: (1) restricted zone of two membranes in apposition, either one or both of which exhibited increased thickness or electron contrast; and (2) the presence of vesicles, 30–50 nm in size, in one or both of the two cytoplasmic domains separated by the opposing membranes. We performed two measures of the length of the axon–spine interfaces. The first one was limited to the active zone (AZ), composed of the synaptic cleft bordered by vesicles on the presynaptic axonal bouton and corresponding to the postsynaptic density (PSD) on the dendritic spine (Schikorski and Stevens, 1997). The second measure, including the active zone, was extended to the nonsynaptic interface, characterized by the thin extracellular space bordered by spine and bouton membranes without specialization. Digital images were analyzed using a computer assisted image analysis system (MCID 7.0; Imaging Res. Inc.). The quantitative analysis was blind with the person doing the analysis unaware of the genotypes of the mice.

All data were exported and converted to a frequency distribution histogram using the Sigma-Plot 8.0 program (SPSS-Erkrath). A paired *t*-test was used to compare DTg and

control groups. A difference was accepted as significant if the probability was less or equal than 5% ($P \leqslant 0.05$). All data are expressed as mean ± S.E.M.

Individual images of control and transgenic mice were assembled and the same adjustments were made for brightness, contrast, and sharpness using Adobe Photoshop (Adobe Systems).

RESULTS

Derivation of conditional *SCA1* transgenic mice

We used the TET system (Furth *et al.*, 1994) to obtain *in vivo* regulatable expression of ATAXIN1 in mouse tissues. This system is well-known and characterized and is enables either induction or suppression of expression of a gene of interest *in vivo*. Modulation of expression is achieved by a combination of specifically interacting prokaryotic sequences inserted in two different elements (Fig. 1a). Transgenic mice with a tetracycline transactivator (tTA)-expressing transgene and a TET-responder transgene (Double transgenic mice, DTg) constitutively express ATAXIN1 protein. The expression is modulated *in vivo* by tetracycline administration/withdrawal.

Production and selection of SCA1 TET-transgenic mice

In one group of transgenic mice the TRE was followed by cDNA encoding a myc-tagged normal ATAXIN1 protein (32 repeats) whereas in another group it was followed by cDNA encoding a myc-tagged expanded ATAXIN1 protein (100 repeats) (Fig. 1b). Founders and transgenic mice were identified by PCR analysis. The integrity of the transgenes was verified by Southern-blot analyses on *EcoR* I digested genomic DNA from transgenic mice. Transgene copy number for each transgenic line was determined by computer analysis (Quantity One Software, Bio-Rad Laboratories) of hybridization signal intensity on Southern blots. The transgenic responder line TRE-nSCA74 (transgene copy number 44–56) and the transgenic responder line TRE-eSCA62 (transgene copy number 2–4) were selected because of high levels of ATAXIN1 expression in the CNS when crossed to a CNS-specific tTA-expressing transgenic line (data not shown).

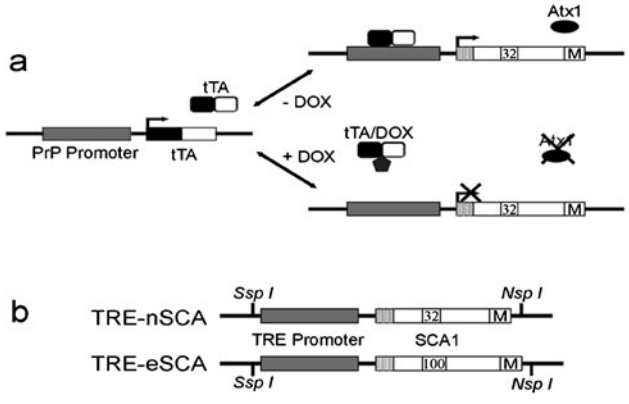

Fig. 1. The binary tetracycline-regulated gene expression system (a) and transgenic constructs (b). Atx1, ataxin-1; DOX, doxycycline; TRE, tetracycline-responsive element; tTA, tetracycline-responsive transactivator.

These two transgenic lines were then crossed with the PrP-tTA transgenic line, which is known to express high levels of tTA mainly in the CNS (Boy *et al.*, 2006).

Analysis of PrP-tTA/TRE-SCA1 DTg mice

PrP-tTA/TRE-SCA1 DTg mice were produced by crossing Dox-treated transgenic females with transgenic males. In the absence of Dox treatment of mothers, DTg embryos died early, which indicates toxicity of ATAXIN1 during mouse embryonic development. To bypass this embryo-lethality and to obtain post-natal expression of ATAXIN1, transgenic activator or responder females were treated with Dox (0.5 mg/ml in 5% sucrose for 1 week before mating, as described in the Methods section).

Transgene expression

To test the time-course of the induction of ATAXIN1 expression, DTg and littermate-control animals were sacrificed at different ages. The *in situ* ATAXIN1 expression was detected by immunohistochemistry at 11-weeks old, following behavioral analyses and phenotypic characterization. Expression of the transgene was scattered throughout the CNS. Considerable levels of transgenic ATAXIN1 were detected in frontal cortex, striatum, hippocampus and cerebellum of DTg animals (Fig. 2a–d). In all CNS regions the expression of the ATAXIN1 colocalizes with the expression of c-myc tag (Fig. 3). Highest expression of the transgene was detected in cerebellar cortex, mainly in Purkinje cell and granular cell layers (Fig. 4a). Confocal analyses of double immunohistochemistry against ATAXIN1 and calbindin D-28k, a specific marker of cerebellar Purkinje cells, were performed to better characterize this expression in cerebellum. In Purkinje cells, the expression of ATAXIN1 is

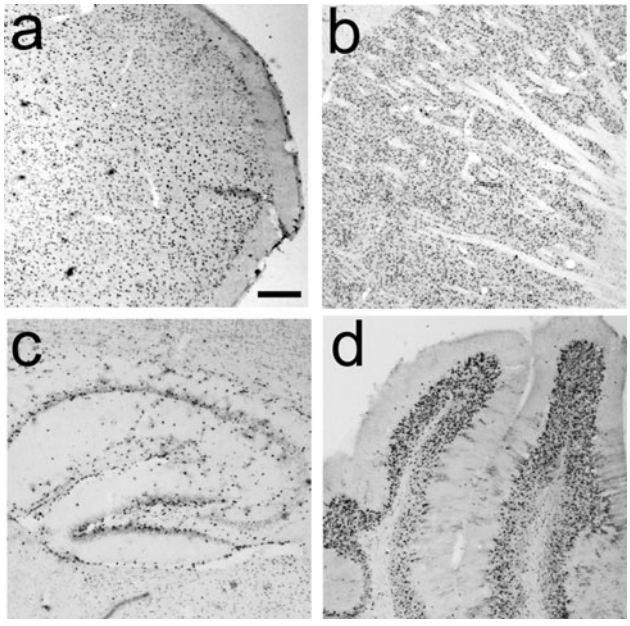

Fig. 2. Ataxin-1 distribution in the brain. (a–d) Brain sections from 11-week-old DTg mice were immunostained with anti-ATAXIN1 (11NQ antibody). Cells positive for ATAXIN1 were scattered in different layers of the frontal cortex (a), widely distributed in the striatum (b), in all hippocampal regions (c) and in the cerebellar cortex (d). Scale bar, 200 μm.

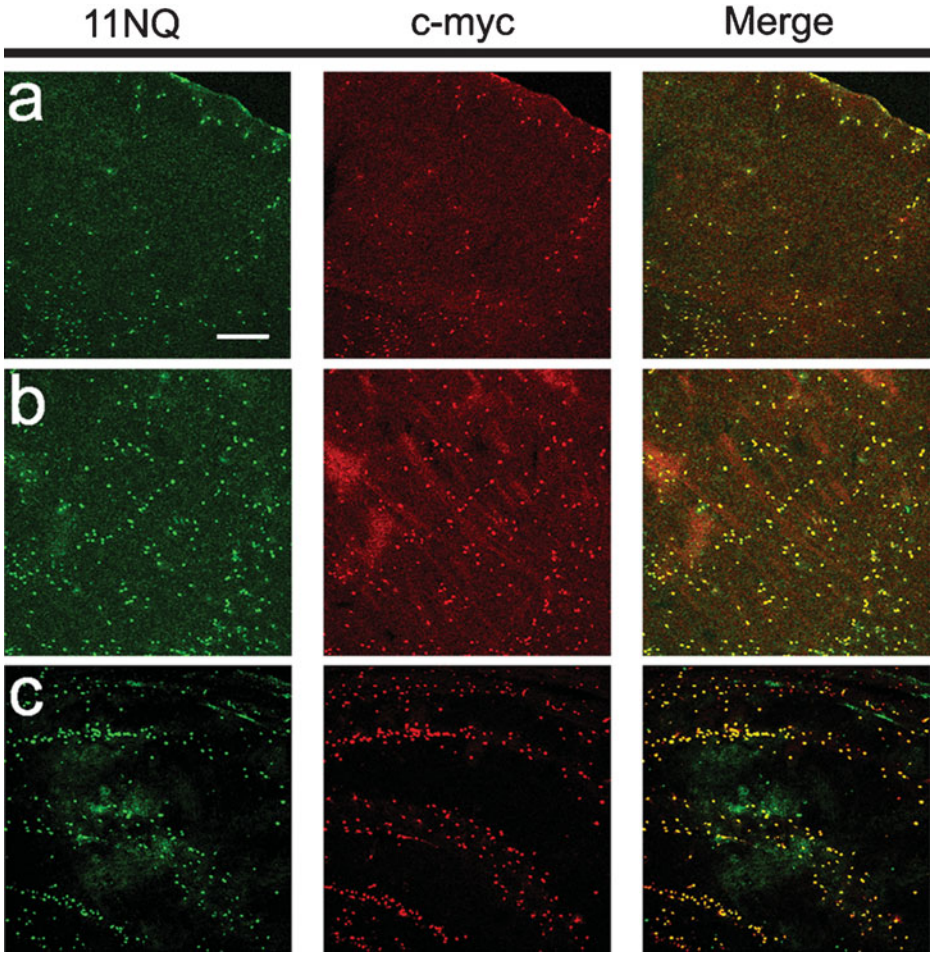

Fig. 3. Mutant ATAXIN1 in brains of DTg mice. (a–c) Most cells that express human ATAXIN1 in the frontal cortex (a), striatum (b) and hippocampus (c) stain for the c-myc tag. Scale bar, 100 μm.

both cytoplasmic and nuclear. Moreover, the morphology of the Purkinje cells appears well preserved, as it will be described in the next section (Fig. 4b). To distinguish between endogenous and transgenic ATAXIN1, double staining for c-myc tag and human ATAXIN1 was performed, which demonstrates colocalization of the signals (Fig. 3c). Western blot and RT-PCR inticates expression in the cerebellum (Fig. 4d,e) and brains of DTg mice. The expression of transgenic ATAXIN1 started in 2-week-old DTg mice and reached the full expression in 3-week-old DTg mice. After this age, RT-PCR analysis of ATAXIN1 mRNA demonstrates that transcription of the transgene remains stable.

Purkinje cell morphology

As revealed by calbindin staining (Fig. 5a,b), the dendrites of Purkinje cells of DTg and control mice appeared normal by confocal microscopy analysis. The spine densities of distal dendrites with an average diameter <1.5 μm were 1.64 ± 0.09 spines per μm (mean ± SD) and 1.76 ± 0.17 spines per μm in 11-week-old DTg mice ($n = 6$) and control ($n = 6$), respectively ($t = 0.65$; $P = 0.58$) (Fig. 5c). Likewise, the spine density in dendritic fragments with an average diameter >1.5 μm (proximal category) (Fig. 5a) was 2.7 ± 0.1 spines per μm in 11-week-old DTg mice and 2.65 ± 0.08 spines per μm in control ($t = -1$; $P = 0.39$) (Fig. 5c). Thus, the spine density of Purkinje cells in DTg mice did not differ significantly from that of control littermates (distal versus distal, $P>0.5$; proximal versus proximal, $P>0.5$; total versus total, $P>0.5$; Student's *t*-test).

In contrast, in 20-week-old DTg mice the dendritic arbor and the number of Purkinje cells are reduced as shown by the calbindin staining of cerebellar cortex (Fig. 5e,g) compared to control mice (Fig. 5d,f).

Neurological alteration in *SCA1* transgenic mice

DTg mice started to show behavioral abnormalities at ~9 weeks of age. Neurological alterations were assayed until 20 weeks after birth (Fig. 6). In a home cage-behavior study, they showed mild dystonic head movements and spatial incoordination during walking. These symptoms worsened progressively during the next week and gait abnormalities started to appear. DTg mice expressing ATAXIN1 also showed a decrease in growth rate starting from 6 weeks of age. This decrease became statistically significant starting from 9 weeks of age compared to control mice ($t = -5.76$, $P = 0.01$ in 9-week-old mice; $t = -10.8$, $P = 0.04$ at the end

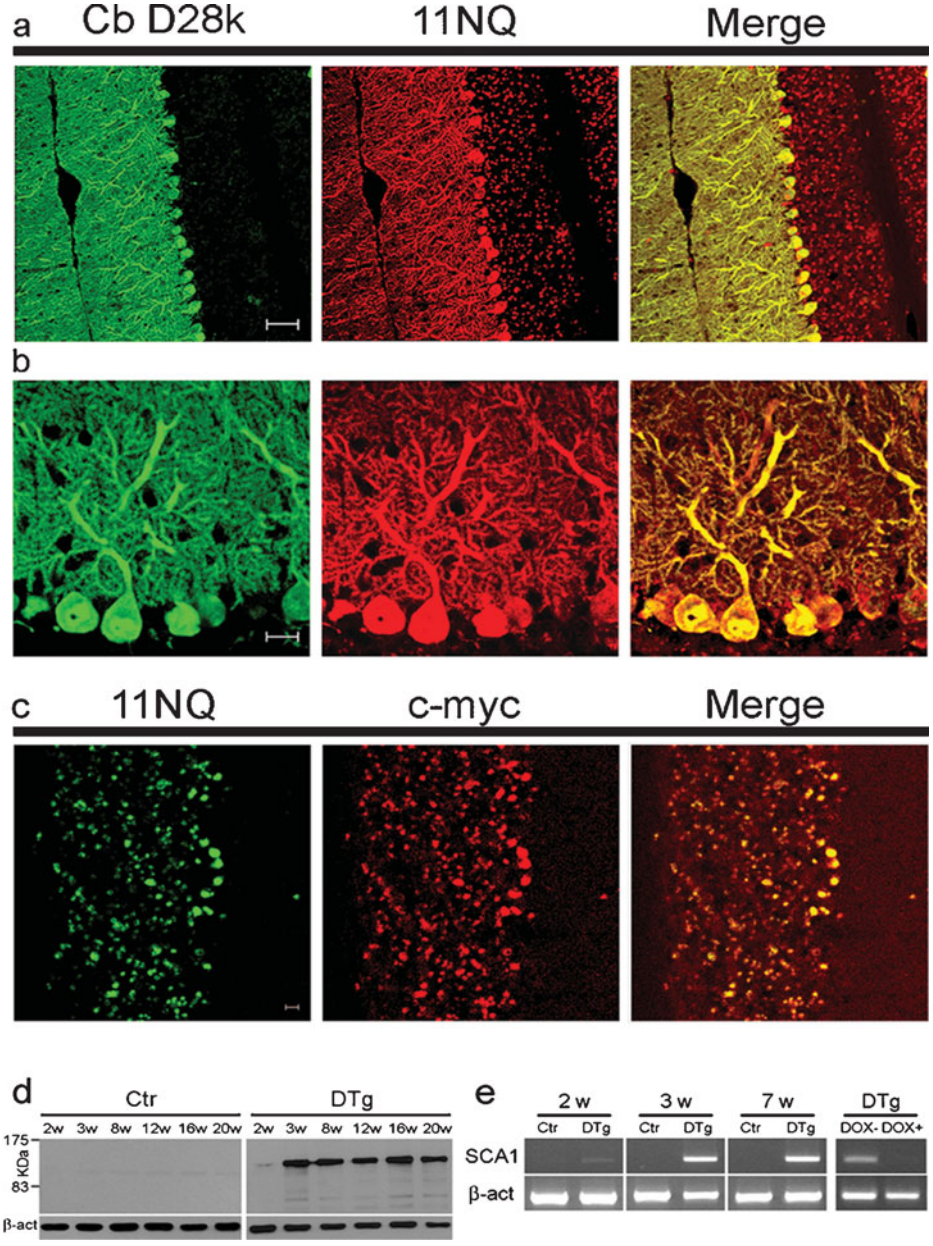

Fig. 4. Transgenic ATAXIN1 is expressed in the cerebellum. (a) Immunolabeling of sagittal sections for transgenic ATAXIN1 show Purkinje cells and granule cells positive for ATAXIN1. Calbindin D-28k (CbD28k)-positive Purkinje cells are positive for ATAXIN1. (b) The morphology of dendritic tree branching and spine distribution is normal in CbD28k-positive Purkinje cells that express ATAXIN1. (c) In a single Z plane of the cerebellar cortex, immunolabeling of transgenic ATAXIN1 colocalizes with expression of the c-myc tag. (d) Western blots showing expression of transgenic ATAXIN1 in the cerebellum of DTg mice. ATAXIN1 is not detected in control mice. (e) RT-PCR analyses of the expression of transgenic ATAXIN1 mRNA in the cerebellum of DTg mice at different ages and in response to DOX treatment. Scale bars, 50 μm in a; 10 μm in b and c.

of the study) (Fig. 7). We performed several motor behavioral tests to further clarify the neurological phenotype of these mice.

Performance in the open-field test

This test is mainly used to study novelty induced exploratory behavior, but it can also used to evaluate locomotor activity (Karl *et al.*, 2003). The number of grids crossing per day/interval was analyzed in 11-week-old mice (Fig. 8a). Following exposure to a novel environment, control mice showed a classic exploratory behavior consisting of a reduced tendency to examine the environment and trying to avoid the bright open area. In the following days, mice got used to the environment and they showed no fear in exploring the environment and walking in the bright fields of the arena. DTg mice showed a different behavior. Even in the first two days of trial there was a significant difference in grid-crossing compared to the control ($F = 7.87$; $P<0.0001$), which was not related to an enhanced ability in exploring the environment. During the days that followed the grid-crossing patterns did not change compared to the first two days. In addition, the mice showed no preference for avoiding bright open fields in the first days. In summary, their behavior in the arena did not change during the trial. They explored the arena without any clue related to the environment: over trials, many times, they recrossed the same grids without exploring the sides of the

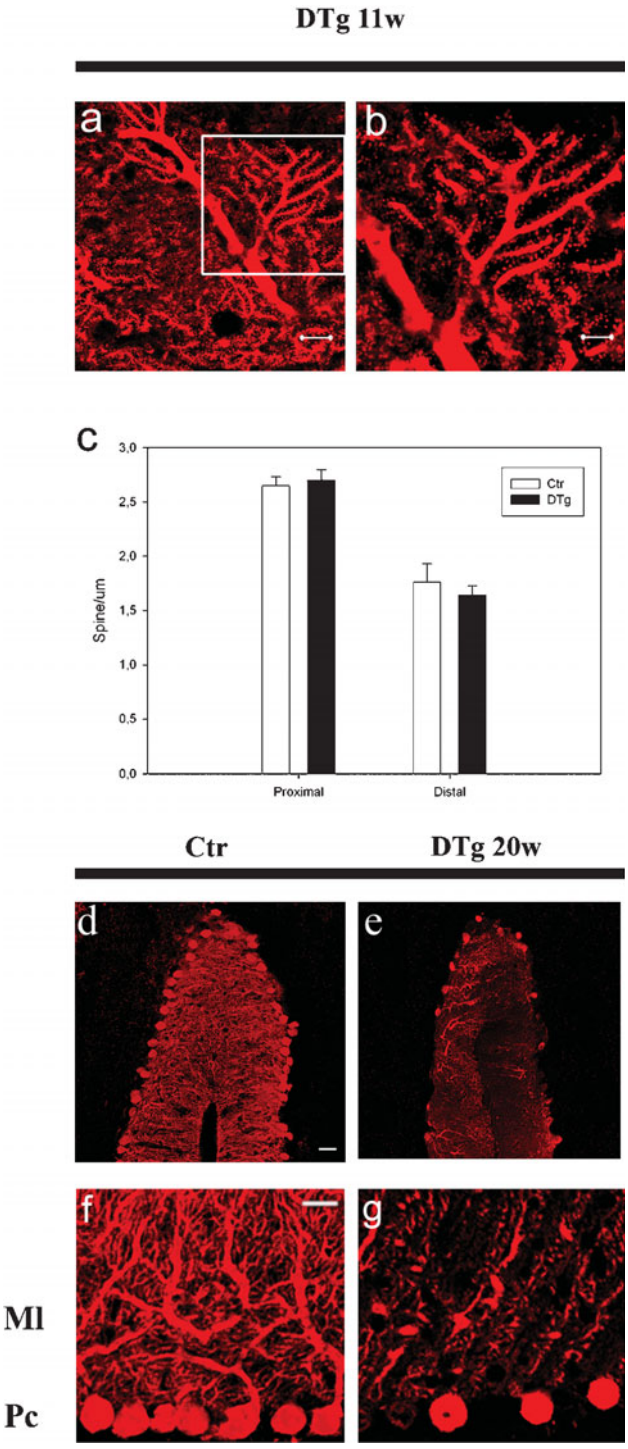

Fig. 5. Purkinje spine density. (a) Confocal microscopy image of a representative plane of the dendritic tree of a Purkinje cell labeled for calbindin D-28k in an 11-week-old DTg mouse. The pattern of ramifications and spine number is normal. (b) The well-preserved spine density is evident in a third-order dendrite. (c) Quantitative analysis of the number of dendritic spines in proximal (average diameter >1.5 μm) (2.65 ± 0.08 and 2.7 ± 0.1) and distal (average diameter <1.5 μm) (1.76 ± 0.17 and 1.64 ± 0.09) dendrites of control and DTg mice, respectively. (d–g) Confocal microscopy at different magnification of a representative region of interest of the cerebellar cortex of labeled for calbindin D-28k in 20-week-old control (Ctr) (d,f) and DTg (e,g) mice. The normal, extensive pattern of dendritic arborization is evident in the sagittal section of the Ctr animal. In DTg mice, at 20 weeks of age, there is a decrease of Purkinje cells and Purkinje cells show a reduced dendritic arborisation,. Abbreviations: Pc, Purkinje cells; Ml, molecular layer. Scale bars, 10 μm in a; 5 μm in b; 50 μm in d; 20 μm in f.

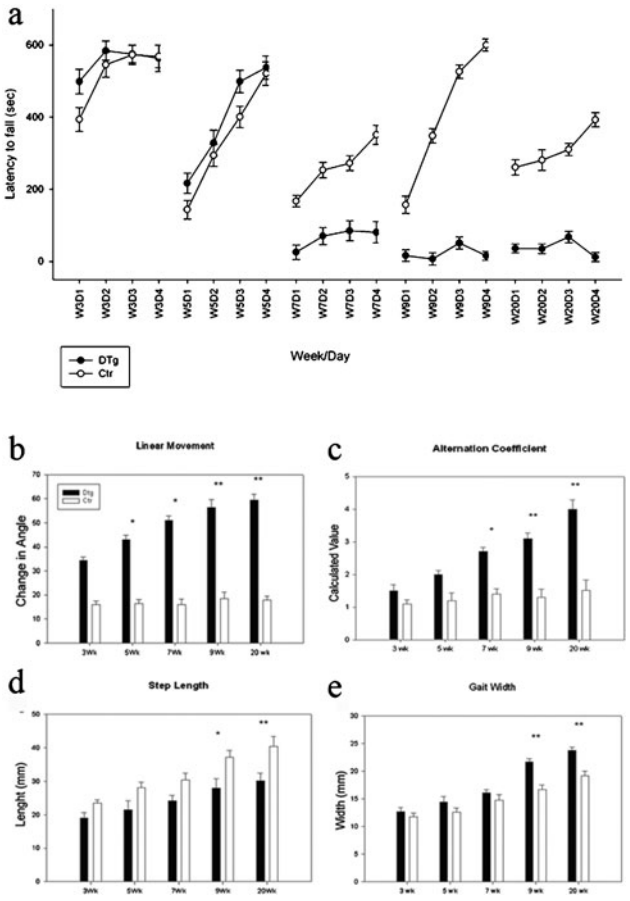

Fig. 6. Neurological assessment during the development of SCA1. (a) Time course of the performances in the rotarod. At 3-weeks old DTg mice (filled circles) fell off sooner than control mice (open circles). The main difference in the rotarod performances is evident at 9-weeks old and remains constant until 20-weeks old. Data are mean ± S.E.M. (b–e) Analysis of gait during progression of SCA1. (b) In linear-movement analysis, DTg mice showed a progressive increase in the linear movement score at 9- and 20-weeks old (56.42 ± 3.15 and 59.5 ± 2.45, respectively) compared to control mice (18.46 ± 2.74 and 17.9 ± 1.65, respectively). (c) In the step alternation coefficient study, DTg mice showed a progressively more shuffling gate with a higher score at 9-weeks old (3.1 ± 0.18) than control animals (1.3 ± 0.25). This difference became greater at 20 weeks (4.0 ± 0.29 and 1.52 ± 0.31, Ctr and DTg, respectively). (d) In DTg mice there was a progressive reduction in step length, which was significantly different to control mice at 9- and 14-weeks old (27.98 ± 2.76 compared to 37.12 ± 2.12, and 30.12 ± 2.25 compared to 40.45 ± 3.01, respectively). (e) In the gait-width analysis there was an increase in gait width in DTg mice compared to control mice. At 9-weeks old the gait width of DTg mice was significantly larger than that of controls (27.7 ± 0.57 compared to 16.68 ± 0.85), and the difference increased at 20-weeks old (23.75 ± 0.58 compared to 19.18 ± 0.78). $^{*}P \leqslant 0.05$; $^{**}P \leqslant 0.01$; $n = 6$; data, mean ± S.E.M.

arena. This indicates lack of spatial coordination in the behavior of these mice. This hypothesis is confirmed by the latency to periphery analysis (Fig. 8b). In control mice the time taken to reach the periphery of the arena decreased in consecutive trials ($F = 10.12$; $P<0.0001$). On the 4th day of trial, placing objects in the arena increased the time taken to reach the periphery but this difference was not significant compared to the first days of the trial. DTg mice showed latency to periphery pattern that does not match with a classic exploratory behavior, because at day 3 they showed no habituation to the environment. At day 4, placing objects in the arena significantly reduced the time to reach the periphery rather than increasing it because of the

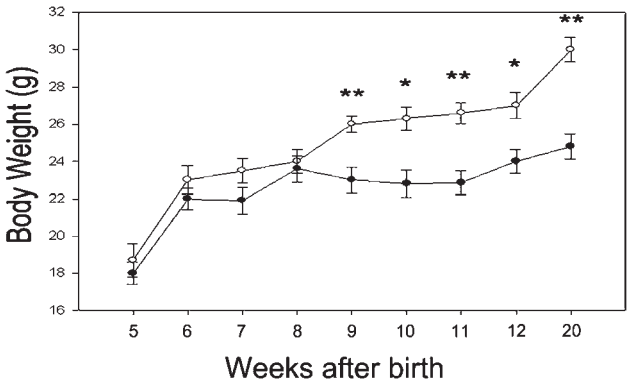

Fig. 7. Growth curves of female DTg mice and control mice. DTg mice that express ATAXIN1 show a progressive reduction in body weight compared to control mice. The difference in body weight between DTg (filled circles) and control mice (open circles) is significant from 9-weeks old. $^{*}P \leqslant 0.05$; $^{**}P \leqslant 0.01$; $n = 4$–6 for each group.

introduction of novel factors into the environment. Together, these data are consistent with spatially uncoordinated behavior in these mice.

Performance on the rotarod

The rotarod measures the ability to maintain balance on a rotarod (Barlow *et al.*, 1996), allowing motor coordination, balance and ataxia to be studied with this test. This task requires intact cerebellar function and motor coordination (Carter *et al.*, 1999). Mice with severe motor coordination problems will have difficulty remaining on the rotarod. In our experiments we used naïve animals to avoid the possibility that learning of the task might affect the motor performance. In this task, 11-week-old DTg mice showed a significant reduction in the latency to fall time. During all four days of trial they fell off earlier than controls. This was significant on days 1 and 3 of the experimental protocol ($F = 14.01$; $P<0.0001$) (Fig. 8c). This pattern remained stable throughout the experimental procedure, which shows that learning the task does not influence the motor performance of the animals and indicates that neurological impairment affects the performance. Most commonly DTg mice fell off close to the end of the first 5 min, showing an inability to keep motor balance and coordination at higher speed rates. During the execution of the task, before falling off the rod, mice had a tendency to hold on to the rod. To analyze the impact of this on rotarod performance in these mice, we examined the total number of holdings on and the total time that mice spent doing so per day/interval (Fig. 8d,e), which revealed that both number of times the mice held on ($F = 177.4$; $P<0.0001$) and time spent holding on ($F = 82.64$; $P<0.0001$) increased progressively over the days of trial. These analyses indicate that mice spent most of the time holding on the rotarod during the final days of trial, and that the reduction in time taken to fall was caused exclusively to an impairment of motor coordination and balance because mice retained the strength to hold the rod.

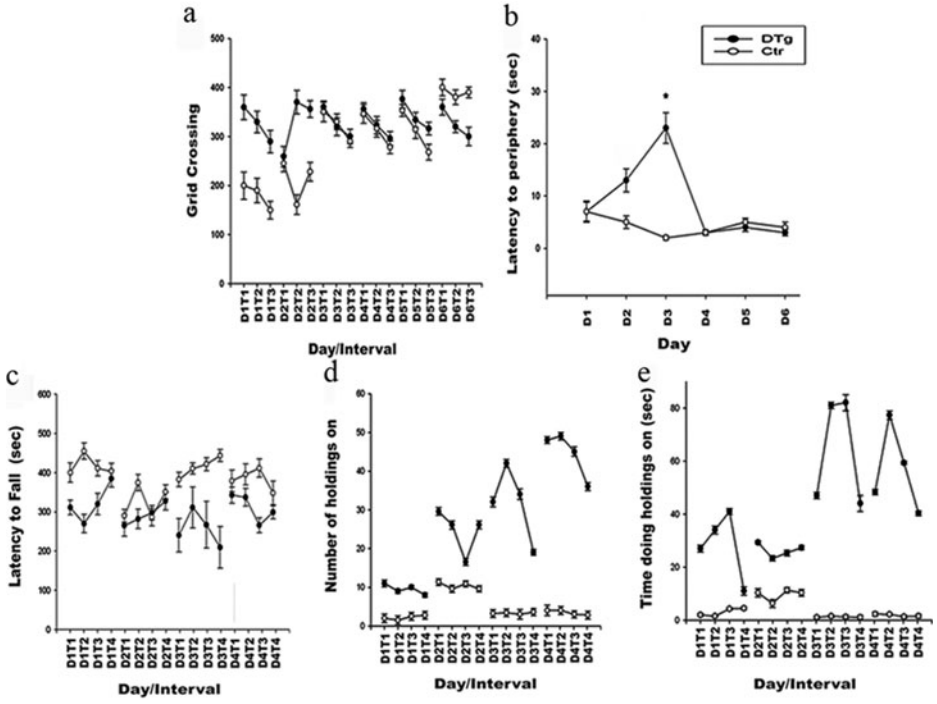

Fig. 8. Behavioral assessment. (a) In the open-field test, the normal exploratory behavior of control mice consisted of an initial reduced tendency to examine the environment followed by avoidance of the bright open area. In the first days of trial, DTg mice have a high rate of grid crossing that is not related to an enhanced ability to explore the environment. This behavior does not change in subsequent days. (b) In control mice the time taken to reach the periphery of the arena gradually decreases. On the 4th day of trial, placing of objects in the arena increased the performance of the mice. The pattern of the change in time taken for DTg mice to reach the periphery does not match with normal exploratory behavior: at day 3 they showed no habituation to the environment, and a spatially uncoordinated behavior ($^{*}P \leqslant 0.05$; $n = 6$ for each group). Data are mean ± S.E.M. (c–e) In the rotarod test DTg mice took significantly less time taken to fall (c) compared to control mice. The number of times DTg mice held on to the rotarod (d) and the total time spent holding on (e) both increased significantly during the course of the trial. These values did not change in control mice. Data are mean ± S.E.M.

Gait abnormalities in DTg mice

To assess whether gait was abnormal in 11-week-old DTg mice, we performed a footprint test that evaluates the walking pattern of mice. Footprint patterns were assayed quantitatively by four measurements: linearity of movement; step alternation coefficient; step length; and gait width (Clark *et al.*, 1997). There was a significant difference in all four parameters in the DTg mice compared to control mice. In the linear movement analysis, the average change in angle between consecutive right-right steps was assayed. In this test, a large linear movement score (Clark *et al.*, 1997) indicates non-linear movement and DTg mice clearly showed this abnormality (Fig. 9a) because they received a score of 57.5 ± 5.0 compared to 17.5 ± 3.5 for controls (t = −14.14; $P = 0.0007$). The step alternation coefficient (Fig. 9b), an indication of the uniformity of step alternation, indicates that DTg mice had a shuffling gate because they scored 3.58 ± 0.3, compared to 1.42 ± 0.2 (t = −0.86; $P = 0.04$) in controls. Step-length analysis also confirmed an ataxic gait in the DTg mice (Fig. 9c), with a score of 27.2 ± 4.2 compared to the score of 36 ± 4 for control mice. This indicates that DTg mice required more steps than controls to cover a fixed travel distance (t = −4.9; $P = 0.04$). In the last study (Fig. 9d), gait-width analysis identified a highly significant difference (t = −8.69; $P = 0.0003$) between DTg and control mice with gait width larger in DTg mice than controls (22.28 ± 2.16 compared to 19.16 ± 1.01). Together, these analyses confirm ataxic gait in DTg mice.

EAAT1 clustering modifies the glutamate uptake apparatus in DTg mice

EAAT1 has a key role in controlling the extracellular concentration of glutamate in the cerebellum, is mainly expressed on astrocyte membranes (Danbolt, 2001). In control mice, EAAT1 expression measured as mean density (Density-ROD) was similar (0.69 ± 0.007) to DTg mice (0.74 ± 0.005) (t = −4.3; $P = 0.001$) (Fig. 10c). EAAT1 is distributed homogeneously over the molecular layer in the cerebellar cortex of control mice (Fig. 10a). In fact, the ratio IOD:SD (18.14 ± 1.84) indicates a very low SD value (t = 2.95; $P = 0.01$) (Fig. 10d). EAAT1 expression changed dramatically in DTg mice, forming clusters in defined areas around the dendritic tree of the Purkinje cells (Fig. 10b) and the ratio IOD:SD (7.04 ± 0.1) indicates a very high SD value (Fig. 10d). This finding is confirmed by RT-PCR analyses of EAAT1 mRNA, which demonstrate that gene expression is unchanged (Fig. 10e). Confocal analyses indicate that in control mice EAAT1 surrounds the Purkinje cell soma (Fig. 11a). By contrast, in DTg mice, the localization of EAAT1 is less defined, with redistribution and clustering of the transporter along the Purkinje cell layer (Fig. 11b). To analyze clearly the spatial distribution of EAAT1 on glial cells and to exclude its expression on neurons we examined serial sections 0.54-μm apart stained for GFAP, CbD28K and EAAT1,

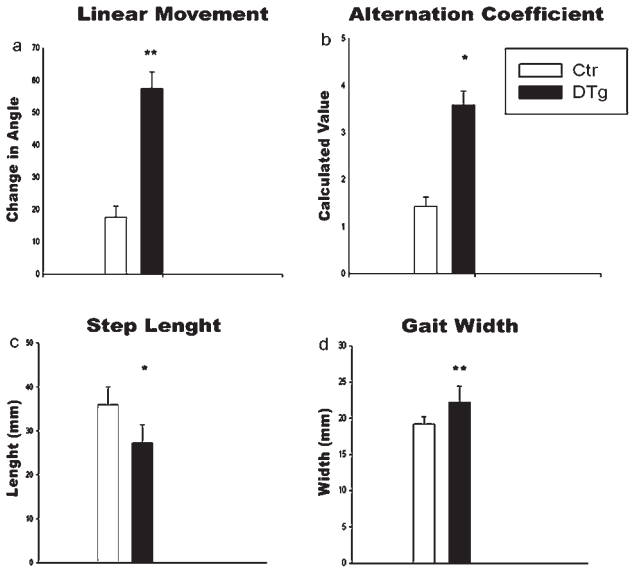

Fig. 9. Analysis of gait. (a) In the linear movement analysis, DTg mice scored higher than control mice (57.5 ± 5 compared to 17.5 ± 3.5). (b) In the step alternation coefficient study DTg mice showed a shuffling gate and achieved a higher score (3.5814 ± 0.3) than control animals (1.4226 ± 0.2). (c) In step-length analysis DTg mice scored higher (27.2 ± 4.2) than control mice (36 ± 4). (d) In gait-width analysis DTg mice had a wider gait (22.2857 ± 2.1647) than controls (19.1667 ± 1.0138). (*$P \leqslant 0.05$; $n = 6$ for each group). Data are mean ± S.E.M.

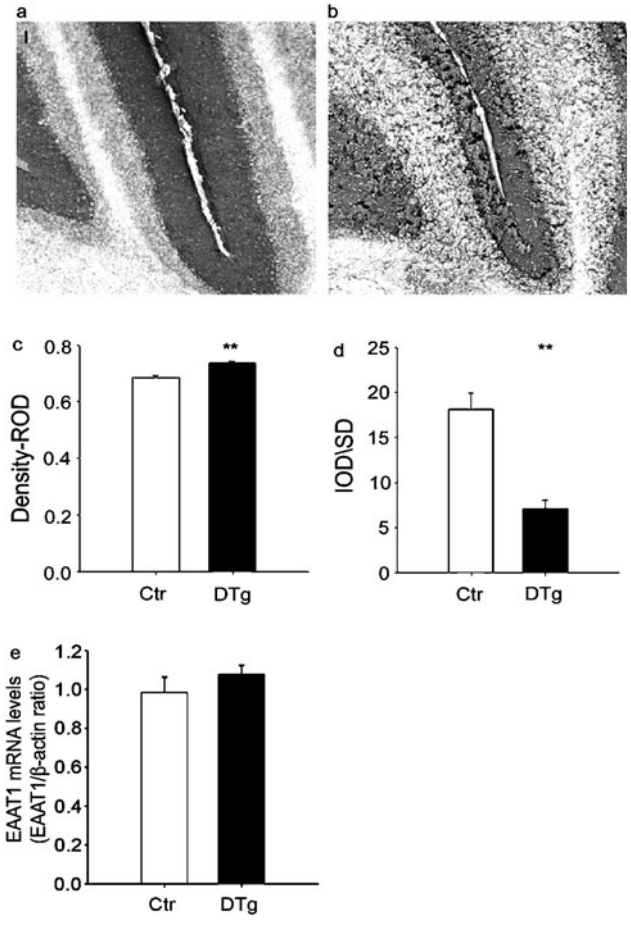

Fig. 10. Clustering of EAAT1 in DTg mice. (a) EAAT1 expression in the cerebellar cortex of control mice appears homogeneous. Scale bar, 50 μm. (b) In DTg mice EAAT1 forms clusters. (c) The total expression in control and DTg mice is similar. (d) The ratio IOD:SD in control mice is high, which indicates homogeneous distribution. The low ratio in DTg mice indicates that the marker is expressed mainly in aggregates. (e) RT-PCR analyses of EAAT1 mRNA confirms that gene expression does not change. **$P \leqslant 0.01$. Data are mean ± S.E.M. Control mice, open columns; DTg mice, filled columns.

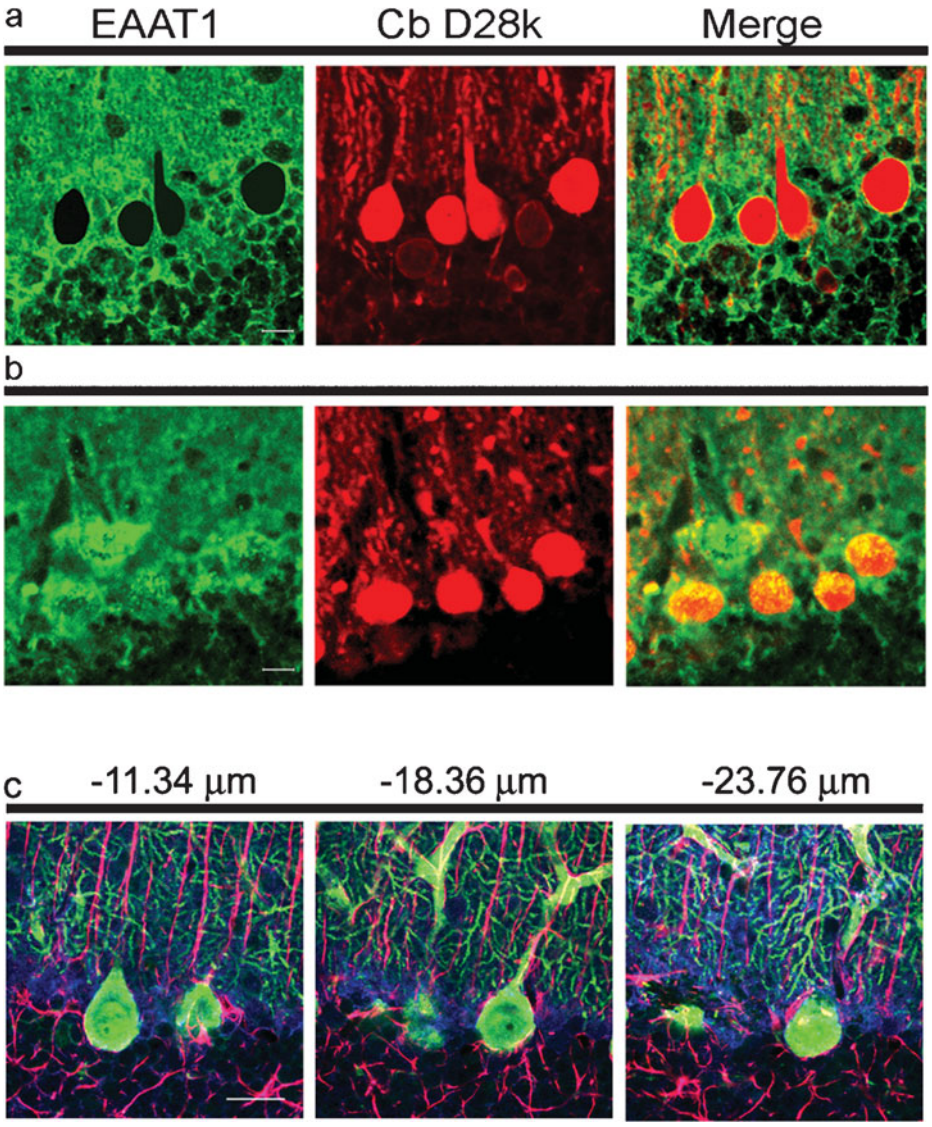

Fig. 11. Clustering of EAAT1. (a) Confocal microscopy of double labeling for EAAT1 and calbindin D-28k confirms that EAAT1 surrounds the Purkinje cell soma and labels the molecular layer homogeneously in control mice. (b) In DTg mice EAAT1 labeling is not homogeneous and appears to coalesce into several clusters. (c) EAAT1 (blue) does not colocalize to the soma of Purkinje cells (green) (−11.34 μm), but covers it (−18.36 μm), outlining the shape of glial processes (GFAP in red) (−23.76 μm). Scale bars: 50 μm in a,b; 20 μm in c.

finding that EAAT1 clusters decorated GFAP-positive cell contours (Fig. 11c).

Evaluation of possible reactive astrocytosis was performed on DTg mice and controls. The reactive astrocytosis was detected using a monoclonal antibody against GFAP, the major glial type III intermediate filament protein. In the cerebellum of DTg mice there was strong GFAP immunoreactivity (0.21 ± 0.01) (Fig. 12b,c) compared to age-matched controls (0.08 ± 0.01) ($t = -5$; $P = 0.00002$) (Fig. 12a,c). These data were confirmed by RT-PCR analyses on total RNA from the cerebellum of DTg mice and controls (Fig. 12d), which revealed an increase in GFAP expression in DTg mice. The reactive astrocytosis represents overexpression of GFAP, which supports an increase of astrocytic-specific intermediate filament causing the transformation of astrocytes from the protoplasmic to the fibrillary type. These cells appear to give rise to several ascending processes that are arranged tightly in a palisade fashion and traverse the molecular layer, which resembles aspects of Bergmann's glia (Altman and Bayer, 1997). In DTg mice, signs of reactive astrocytosis are apparent only in the cerebellum, although ATAXIN1 is expressed in other areas of the brain.

Reactive astrocytosis is associated with EAAT1 clustering

To evaluate the role of reactive astrocytosis in the rearrangement of EAAT1 we surgically injured the cerebellar cortex (Ajtai and Kalman, 1998) and we analyzed the glial reaction 4 days later. GFAP immunopositivity of Bergmann glia appeared to increase in the lesioned area (Fig. 13a,c) and EAAT1 immunopositivity increased with a patchy distribution in the area of the reactive astrocytosis. In contrast, in control mice the level of GFAP is low and EAAT1 staining homogenous (Fig. 13b). These results indicate that resident Bergmann glia are the main component of the glial

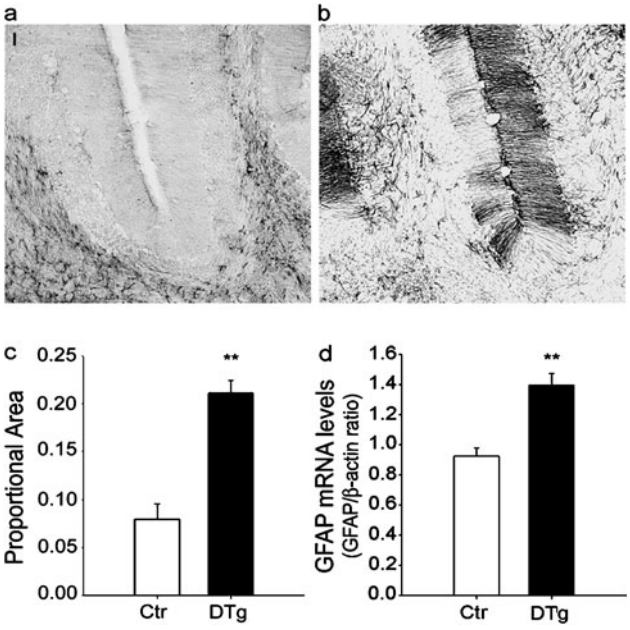

Fig. 12. GFAP expression indicates reactive astrocytosis. (a) GFAP immunoreactivity in the cerebellum of control mice is low. Scale bar, 50 μm. (b) In DTg mice, GFAP expression is strong in Bergmann glia in the cerebellar cortex. (c) In mice that express transgenic ATAXIN1 (filled column), reactive astrocytosis measured as the proportional area labeled for GFAP is higher (0.21 ± 0.01) than age-matched controls (open column) (0.08 ± 0.01). (d) RT-PCR analyses of total RNA confirms the increase in GFAP expression in DTg mice (filled column) compared to controls (open column). $^{**}P \leqslant 0.01$. Data are mean ± S.E.M. DTg mice, filled column; control mice, open column.

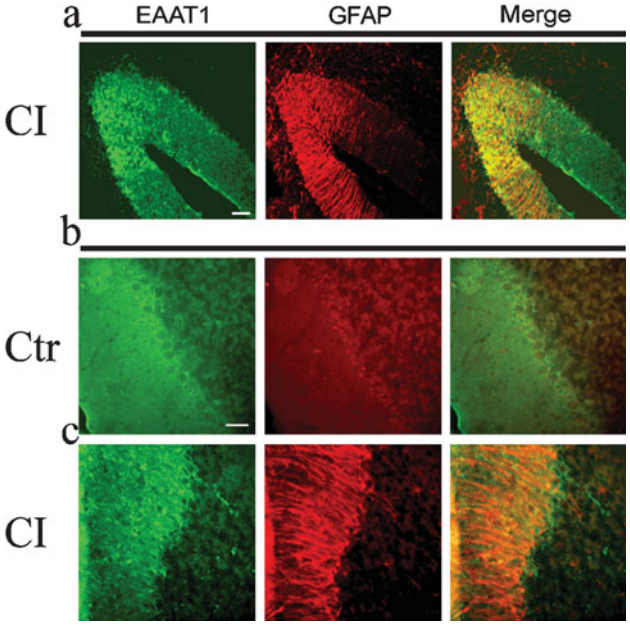

Fig. 13. Correlation between reactive astrocytosis and EAAT1 redistribution in FVB mice at age 2.5–3 months. (a) GFAP immunoreactivity increases on Bergmann glia in the lesioned area. There is no demarcation of the molecular layer, unlike the usual appearance of reactive astrocytosis, which is observed in the granular layer and in the white matter. In the area of cerebellar cortex affected by reactive astrocytosis redistribution of EAAT1 into clusters correlates with over-expression of GFAP in astroglia. (b,c) Higher magnification showing the normal distribution of GFAP and EAAT1 labeling in the cerebellar cortex of control mice (b) and the altered pattern in a mouse with a cerebellar injury (CI). Scale bars, 50 μm in a; 20 μm in b,c.

reaction, and that upregulation of GFAP expression in this highly developed glial architecture is associated with glial cell hypertrophy and rearrangement of distribution of EAAT1 on glial membranes, which results in clustering of this amino acid transporter.

Reduction of the axon–spine interface interferes with uptake and dilution of glutamate in the extracellular space

The axon–spine interface includes both synaptic and non-synaptic components (Fig. 14a,b). The non-synaptic interface has a key role in synaptic function; it is engaged in neuronal glutamate transport and endocytosis, whereas the non-synaptic area constitutes a channel through which molecules might escape from the synaptic cleft, spilling over to neighboring neurons and astrocytes (Ventura and Harris, 1999). In DTg mice, the number of cerebellar synapses in the contact zone (which includes synaptic and non-synaptic interface) is reduced by 20% compared to controls (0.32 ± 0.02 and 0.40 ± 0.02, respectively; $t = -1.14$; $P = 0.04$) (Fig. 14c). The length of the active zone of cerebellar synapses is similar in DTg (0.22 ± 0.01) and control mice (0.22 ± 0.02) ($t = -1.13$; $P = 0.05$) (Fig. 14d). Therefore, we infer that the reduction occurs exclusively in the synaptic interface compartment at the side of the postsynaptic density area, and that this constitutes the very early changes that are accountable for the behavioral phenotype.

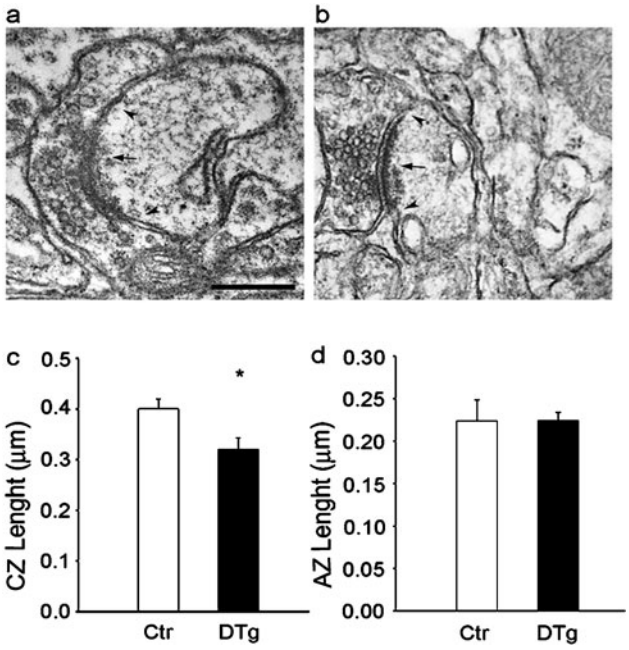

Fig. 14. Changes in synaptic structure. (a) The axon–spine interface includes synaptic (arrow) and non-synaptic components (arrowhead). Scale bar, 0.3 μm. (b) The contact zone, including the synaptic (arrow) and non-synaptic (arrowhead) interface is reduced in DTg mice. (c) In DTg mice the total length of cerebellar synapses (0.32 ± 0.02) is reduced significantly ($P = 0.04$) compared to control mice (0.40 ± 0.02). (d) The active zone length (postsynaptic density) of the cerebellar synapses is the same in DTg (0.22 ± 0.01) and control mice (0.22 ± 0.02). DTg mice, filled columns; control mice, open columns.

CONCLUSIONS

- Using this model we have demonstrated that ATAXIN1, which is expressed ubiquitously in the CNS, is associated with cerebellar motor deficits.
- In the cerebellum, we identified peculiar clustering of the EAAT1glutamate transporter, a significant reduction in the synaptic interface compartment beside the postsynaptic density area, and reactive astrocytosis (GFAP upregulation).
- We consider it likely that these early alterations in cerebellar tripartite synapses lead to the main feature of this neurodegenerative disease: the death of Purkinje cells.

DISCUSSION

Several animal models of SCA1 have been generated using a PcP-2 expression cassette (Vandaele *et al.*, 1991) to drive expression of human mutant ATAXIN1 mainly in Purkinje cells. This approach has identified several steps in the pathogenesis of SCA1 and provided fundamental information about Purkinje disease progression, one of the cerebellar components of the human disease. However, this approach restricts the onset and progression of experimental disease to this type of brain cells. In an alternative approach, Watase *et al.* (2002) have inserted a long CAG repeat in the murine endogenous *Sca1* locus, which mimics the human pathology, to investigate this Purkinje cell disease in a more complex context. Our model reproduces the human features of *ATAXIN1* expression, which allows us to investigate changes in cerebellar circuitry caused when different cells express the mutant protein. The expression of ATAXIN1 occurs in cells other than Purkinje cells, including neurons in the cerebellar granular layer. In our study, the complete rescue of embryonic lethality by administering DOX to the mothers before mating demonstrates the efficiency of DOX-dependent activation of tTA. Moreover, the embryonic phenotype observed in this SCA1 model indicates that expression of mutant *ATAXIN1* during embryonic development increases the severity of the disease, as reported recently by others (Serra *et al.*, 2006). The first appearance of *ATAXIN1* mRNA is detected in 2-week-old DTg mice. The maximum concentration of mRNA and protein occurs at 3 weeks of age in the DTg mice. This highlights a gap between the exposure of the nervous tissues to ATAXIN1 and the onset of symptoms (at 9–10 weeks), which is consistent with other genetically modified models of polyQ diseases (Zu *et al.*, 2004). In this model of ataxia, the combination of motor imbalance and spatial incoordination in the absence of muscle weakness indicates that motor deficits might be related to cerebellar dysfunction. The phenotype of this SCA1 mouse model parallels that of another SCA1 mouse model that has been reported previously (Clark *et al.*, 1997). Our results show early changes in the absence of significant Purkinje cell pathology. The expression and spatial distribution of EAAT1, a glial glutamate transporter (Danbolt, 2001) with key roles in neuron–glia interaction (Watanabe, 2002) and in other neurodegenerative diseases (Ikegaya *et al.*, 2002), is disarranged in our study, presenting with a cluster-like appearance in DTg mice. This finding indicates a that there is a change in glutamate signaling, which is in accordance with microarray studies that report alteration of the expression of genes that encode proteins involved in glutamate signaling pathways in Purkinje cells (Serra *et al.*, 2004). It is possible to envisage two scenarios: either the change in localization of EAAT1 is caused by local changes in glutamate concentration; or EAAT1 distribution is part of a reactive astrocytosis-related response. In a chronic constriction injury model in mice we have reported the appearance of reactive astrocytosis associated with a strong reduction in glial transporters for glycine and glutamate, and a net increase of both these neurotransmitters. These changes might represent the basis of the morphological and functional changes that sustain central plasticity via NMDA receptors (Cavaliere *et al.*, 2008). Experiments in which we injured the cerebellum directly indicate that reactive astrocytosis of Bergman's radial glia, which differs from common reactive reactive astrocytosis as reported by Ajtai and Kalman (1998), induces spatial redistribution of EAAT1. These data are related to the remarkable change identified in our model: the reduction of the non-synaptic area at the axon–spine interface. This provides a channel through which molecules might escape from the synaptic cleft, spill-over to neighboring neurons and astrocytes and reduce synaptic input specificity. Whether a particular synapse will sense the glutamate that escapes from the perimeter of its neighbor depends on uptake and dilution in the extracellular space between them. Because most of the neighboring synapses occur on different presynaptic boutons, glutamate that diffuses between them will reduce input specificity. In the cerebellum of DTg mice, and related to these two early changes, we found overexpression of the astrocytic intermediate filament protein GFAP in Bergmann's glia. According to data from the first mouse model of SCA1 (Burright *et al.*, 1995), reactive astrocytosis was observed in association with the degeneration of Purkinje cells. In our model, although the DTg mice developed motor impairments, no clear signs of cellular degeneration were detected, which indicates that the reactive astrocytosis observed in our model was probably not caused by degeneration of Purkinje cells but to a state of suffering in these cells. In addition, in another mouse model of polyQ syndrome it has been reported that neuronal dysfunction precedes any evident neuronal degeneration (Adachi *et al.*, 2001). Moreover, inflammation of activated glia in most CNS pathologies contributes to neuronal cell death (Bal-Price and Brown, 2001). The location and distribution of astrocytic processes are important for regulating the extracellular milieu in the CNS. Glia occupy 50% of the total volume of the brain (Peters *et al.*, 1991), and glial volume correlates with the number of synapses (Anderson *et al.*, 1994) but glial processes are not uniformly distributed. In fact, in the cerebellar cortex, most of the parallel and climbing fiber synapses are ensheathed by processes of the Bergmann glia that express EAAT1 (Spacek, 1985), forming several independent compartments that control glutamate concentration and interact autonomously with the particular groups of synapses they ensheath (Grosche *et al.*, 1999). The structural relationships between astrocytes and synapses can change in response to glutamate and with altered neuronal function (Carmignoto, 2000). Astrocytes modulate the formation and efficacy of synapses (Smith, 1998), and regulate extracellular glutamate via glutamate transporters. By clearing excess glutamate from the extracellular space, astrocytes protect against excitotoxic glutamate concentrations that might lead to neuronal cell

death (Rothstein, 1996). Recently it has become clear that a change in glial properties is the key trigger that causes synaptic perturbation in several neuropathic disorders (Watkins and Maier, 2003).

Together, our results indicate that, as in other transgenic models of CAG repeat diseases, expression of ATAXIN1 is followed by the onset and progression of motor deficits that might be related directly to cerebellar dysfunction of both Purkinje cells and Bergmann glia. In this regard, neuronal degeneration might be the ultimate step of the neuropathology, when rescue from the disease is no longer possible. Recently, this hypothesis has been partly confirmed by showing that dysfunction of Purkinje cells associated specifically with precise mutation of K^+ channels causes cerebellar ataxia (Shakkottai *et al.*, 2004; Sausbier *et al.*, 2004). By contrast, a complex neurological disorder like SCA1 where cerebellar ataxia is only one component of the disease might be associated with multiple cellular dysfunctions within the cerebellum, as indicated by our study. Although more studies are needed to clarify this assumption, we propose that this conditional mouse model is a key tool with which to identify different steps in the pathology of SCA1 because modulating the expression of the transgene makes it possible to correlate each of these steps with expression ATAXIN1. Our findings provide evidence that this mouse model exhibits features of inflammatory pathology and that it might be useful for studying the role of inflammatory pathways in CAG triplet diseases. Moreover, Colangelo *et al.* (2008), have reported a novel, crucial role of intrathecal administration of nerve growth factor as a strong modulator of plasticity in the neuronal–glial network by reducing reactive astrocytosis. Therefore, our model might also provide a new approach for testing glial-specific drugs that are designed to reduce CNS inflammatory process in the hope of curing this devastating disease.

ACKNOWLEDGEMENTS

We wish to express our gratitude to M. Palomba and A. De Simone for helping in electron microscopy procedures. This work was supported by grants from the Italian Minister of Research and University (PRIN2002 to M.P. and M.L., and DD 21.09.99, n462 ric to M.L.), Italian Telethon Foundation (Grant #GSP010316 to R.G.), Regione Campania (Prog. Spec art 12 E.F. 2000 to M.P. and RF2002 to M.L.), the CNR (Neurobiotecnologie 2003 to M.P.), Regione Campania (L.R. N.5 Bando 2003 to M.P.). M.R. Bianco was supported by a postdoctoral fellowship from the Associazione Levi-Montalcini.

STATEMENT OF INTERESTS

None.

REFERENCES

Adachi H., Kume A., Li M., Nakagomi Y., Niwa H., Do J. *et al.* (2001) Transgenic mice with an expanded CAG repeat controlled by the human AR promoter show polyglutamine nuclear inclusions and neuronal dysfunction without neuronal cell death. *Human Molecular Genetics* 10, 1039–1048.

Ajtai B.M. and Kalman M. (1998) Glial fibrillary acidic protein expression but no glial demarcation follows the lesion in the molecular layer of cerebellum. *Brain Research* 802, 285–288.

Altman J. and Bayer S.A. (1997) Basic cellular organization and circuitry of the cerebellar cortex. In Altman J. and Bayer S.A. (eds) *Development of the Cerebellar System in Relation to its Evolution, Structure, and Functions.* CRC Press, pp. 26–43.

Anderson B.J., Li X., Alcantara A.A., Isaacs K.R., Black J.E. and Greenough W.T. (1994) Glial hypertrophy is associated with synaptogenesis following motor-skill learning, but not with angiogenesis following exercise. *Glia* 11, 73–80.

Bal-Price A. and Brown G.C. (2001) Inflammatory neurodegeneration mediated by nitric oxide from activated glia-inhibiting neuronal respiration, causing glutamate release and excitotoxicity. *Journal of Neuroscience* 21, 6480–6491.

Banfi S., Servadio A., Chung M.Y., Kwiatkowski T.J. Jr, McCall A.E., Duvick L.A. *et al.* (1994) Identification and characterization of the gene causing type 1 spinocerebellar ataxia. *Nature Genetics* 7, 513–520.

Barlow C., Hirotsune S., Paylor R., Liyanage M., Eckhaus M., Collins F. *et al.* (1996) Atm-deficient mice: a paradigm of ataxia telangiectasia. *Cell* 86, 159–171.

Bodner R.A., Outeiro T.F., Altmann S., Maxwell M.M., Cho S.H., Hyman B.T. *et al.* (2006) Pharmacological promotion of inclusion formation: a therapeutic approach for Huntington's and Parkinson's diseases. *Proceedings of the National Academy of Sciences of the U.S.A.* 103, 4246–4251.

Boy J., Leergaard T.B., Schmidt T., Odeh F., Bichelmeier U., Nuber S. *et al.* (2006) Expression mapping of tetracycline-responsive prion protein promoter: digital atlasing for generating cell-specific disease models. *Neuroimage* 33, 449–462.

Burright E.N., Clark H.B., Servadio A., Matilla T., Feddersen R.M., Yunis W.S. *et al.* (1995) SCA1 transgenic mice: a model for neurodegeneration caused by an expanded CAG trinucleotide repeat. *Cell* 82, 937–948.

Carmignoto G. (2000) Reciprocal communication systems between astrocytes and neurones. *Progress in Neurobiology* 62, 561–581.

Carter R.J., Lione L.A., Humby T., Mangiarini L., Mahal A., Bates G.P. *et al.* (1999) Characterization of progressive motor deficits in mice transgenic for the human Huntington's disease mutation. *Journal of Neuroscience* 19, 3248–3257.

Cavaliere C., Cirillo G., Bianco M.R., Rossi F., De Novellis V., Maione S. *et al.* (2008) Gliosis alters expression and uptake of spinal glial amino acid transporters in a mouse neuropathic pain model. *Neuron Glia Biology* 3, 1–14.

Chaudhry F.A., Lehre K.P., van Lookeren C.M., Ottersen O.P., Danbolt N.C. and Storm-Mathisen J. (1995) Glutamate transporters in glial plasma membranes: highly differentiated localizations revealed by quantitative ultrastructural immunocytochemistry. *Neuron* 15, 711–720.

Chen H.K., Fernandez-Funez P., Acevedo S.F., Lam Y.C., Kaytor M.D., Fernandez M.H. *et al.* (2003) Interaction of Akt-phosphorylated ataxin-1 with 14-3-3 mediates neurodegeneration in spinocerebellar ataxia type 1. *Cell* 113, 457–468.

Clark H.B., Burright E.N., Yunis W.S., Larson S., Wilcox C., Hartman B. *et al.* (1997) Purkinje cell expression of a mutant allele of SCA1 in transgenic mice leads to disparate effects on motor behaviors, followed by a progressive cerebellar dysfunction and histological alterations. *Journal of Neuroscience* 17, 7385–7395.

Colangelo A.M., Bianco M.R., Vitagliano L., Cavaliere C., Cirillo G., De Gioia L. *et al.* (2008) A new nerve growth factor (NGF)-mimetic peptide active on neuropathic pain in rats. *Journal of Neuroscience* 28, 2698–2709.

Cummings C.J., Orr H.T. and Zoghbi H.Y. (1999) Progress in pathogenesis studies of spinocerebellar ataxia type 1. *Philosophical transactions of the Royal Society of London. Series B, Biological Sciences* 354, 1079–1081.

Cummings C.J., Sun Y., Opal P., Antalffy B., Mestril R., Orr H.T. *et al.* (2001) Over-expression of inducible HSP70 chaperone suppresses neuropathology and improves motor function in SCA1 mice. *Human Molecular Genetics* 10, 1511–1518.

Custer S.K., Garden G.A., Gill N., Rueb U., Libby R.T., Schultz C. *et al.* (2006) Bergmann glia expression of polyglutamine-expanded ataxin-7 produces neurodegeneration by impairing glutamate transport. *Nature Neuroscience* 9, 1302–1311.

Danbolt N.C. (2001) Glutamate uptake. *Progress in Neurobiology* 65, 1–105.

Davies S.W., Turmaine M., Cozens B.A., DiFiglia M., Sharp A.H., Ross C.A. *et al.* (1997) Formation of neuronal intranuclear inclusions underlies the neurological dysfunction in mice transgenic for the HD mutation. *Cell* 90, 537–548.

DiFiglia M., Sapp E., Chase K.O., Davies S.W., Bates G.P., Vonsattel J.P. *et al.* (1997) Aggregation of huntingtin in neuronal intranuclear inclusions and dystrophic neurites in brain. *Science* 277, 1990–1993.

Emamian E.S., Kaytor M.D., Duvick L.A., Zu T., Tousey S.K., Zoghbi H.Y. *et al.* (2003) Serine 776 of ataxin-1 is critical for polyglutamine-induced disease in SCA1 transgenic mice. *Neuron* 38, 375–387.

Fernandez-Funez P., Nino-Rosales M.L., de Gouyon B., She W.C., Luchak J.M., Martinez P. *et al.* (2000) Identification of genes that modify ataxin-1-induced neurodegeneration. *Nature* 408, 101–106.

French S.J. and Totterdell S. (2004) Quantification of morphological differences in boutons from different afferent populations to the nucleus accumbens. *Brain Research* 1007, 167–177.

Furth P.A., St O.L., Boger H., Gruss P., Gossen M., Kistner A. *et al.* (1994) Temporal control of gene expression in transgenic mice by a tetracycline-responsive promoter. *Proceedings of the National Academy of Sciences of the U.S.A.* 91, 9302–9306.

Ginsberg S.D., Martin L.J. and Rothstein J.D. (1995) Regional deafferentation down-regulates subtypes of glutamate transporter proteins. *Journal of Neurochemistry* 65, 2800–2803.

Gossen M. and Bujard H. (1992) Tight control of gene expression in mammalian cells by tetracycline-responsive promoters. *Proceedings of the National Academy of Sciences of the U.S.A.* 89, 5547–5551.

Griffin W.S., Liu L., Li Y., Mrak R.E. and Barger S.W. (2006) Interleukin-1 mediates Alzheimer and Lewy body pathologies. *Journal of Neuroinflammation* 3, 5.

Grosche J., Matyash V., Moller T., Verkhratsky A., Reichenbach A. and Kettenmann H. (1999) Microdomains for neuron-glia interaction: parallel fiber signaling to Bergmann glial cells. *Nature Neuroscience* 2, 139–143.

Ikegaya Y., Matsuura S., Ueno S., Baba A., Yamada M.K., Nishiyama N. *et al.* (2002) Beta-amyloid enhances glial glutamate uptake activity and attenuates synaptic efficacy. *Journal of Biological Chemistry* 277, 32180–32186.

Ishiguro H., Yamada K., Sawada H., Nishii K., Ichino N., Sawada M. *et al.* (2001) Age-dependent and tissue-specific CAG repeat instability occurs in mouse knock-in for a mutant Huntington's disease gene. *Journal of Neuroscience Research* 65, 289–297.

Karl T., Pabst R. and von Horsten S. (2003) Behavioral phenotyping of mice in pharmacological and toxicological research. *Experimental Toxicology and Pathology* 55, 69–83.

Klement I.A., Skinner P.J., Kaytor M.D., Yi H., Hersch S.M., Clark H.B. *et al.* (1998) Ataxin-1 nuclear localization and aggregation: role in polyglutamine-induced disease in SCA1 transgenic mice. *Cell* 95, 41–53.

Lehre K.P. and Danbolt N.C. (1998) The number of glutamate transporter subtype molecules at glutamatergic synapses: chemical and stereological quantification in young adult rat brain. *Journal of Neuroscience* 18, 8751–8757.

Lorenzetti D., Watase K., Xu B., Matzuk M.M., Orr H.T. and Zoghbi H.Y. (2000) Repeat instability and motor incoordination in mice with a targeted expanded CAG repeat in the Sca1 locus. *Human Molecular Genetics* 9, 779–785.

Mrak R.E. and Griffin W.S. (2005) Glia and their cytokines in progression of neurodegeneration. *Neurobiology of Aging* 26, 349–354.

Okuda T., Hattori H., Takeuchi S., Shimizu J., Ueda H., Palvimo J.J. *et al.* (2003) PQBP-1 transgenic mice show a late-onset motor neuron disease-like phenotype. *Human Molecular Genetics* 12, 711–725.

Orr H.T. and Zoghbi H.Y. (2007) Trinucleotide repeat disorders. *Annual Reveiw of Neuroscience* 30, 575–621.

Papa M., Boscia F., Canitano A., Castaldo P., Sellitti S., Annunziato L. *et al.* (2003) Expression pattern of the ether-a-gogo-related (ERG) K+ channel-encoding genes ERG1, ERG2, and ERG3 in the adult rat central nervous system. *Journal of Comparative Neurology* 466, 119–135.

Papa M., Bundman M.C., Greenberger V. and Segal M. (1995) Morphological analysis of dendritic spine development in primary cultures of hippocampal neurons. *Journal of Neuroscience* 15, 1–11.

Paulson H.L. (1999) Protein fate in neurodegenerative proteinopathies: polyglutamine diseases join the (mis)fold. *American Journal of Human Genetics* 64, 339–345.

Peters A., Palay S.L. and Webster H.deF. (1991). *The Fine Structure of the Nervous System.* Oxford University Press.

Rimoldi M., Servadio A. and Zimarino V. (2001) Analysis of heat shock transcription factor for suppression of polyglutamine toxicity. *Brain Research Bulletin* 56, 353–362.

Robitaille Y., Schut L. and Kish S.J. (1995) Structural and immunocytochemical features of olivopontocerebellar atrophy caused by the spinocerebellar ataxia type 1 (SCA-1) mutation define a unique phenotype. *Acta Neuropathologica* 90, 572–581.

Rothstein J.D. (1996) Excitotoxicity hypothesis. *Neurology* 47, S19–S25.

Rozen S. and Skaletsky H. (2000) Primer3 on the WWW for general users and for biologist programmers. *Methods in Molecular Biology* 132, 365–386.

Saulle E., Gubellini P., Picconi B., Centonze D., Tropepi D., Pisani A. *et al.* (2004) Neuronal vulnerability following inhibition of mitochondrial complex II: a possible ionic mechanism for Huntington's disease. *Molecular and Cellular Neuroscience* 25, 9–20.

Sausbier M., Hu H., Arntz C., Feil S., Kamm S., Adelsberger H. *et al.* (2004) Cerebellar ataxia and Purkinje cell dysfunction caused by Ca2+-activated K+ channel deficiency. *Proceedings of the National Academy of Sciences of the U.S.A.* 101, 9474–9478.

Schikorski T. and Stevens C.F. (1997) Quantitative ultrastructural analysis of hippocampal excitatory synapses. *Journal of Neuroscience* 17, 5858–5867.

Schols L., Bauer P., Schmidt T., Schulte T. and Riess O. (2004) Autosomal dominant cerebellar ataxias: clinical features, genetics, and pathogenesis. *Lancet Neurology* 3, 291–304.

Serra H.G., Byam C.E., Lande J.D., Tousey S.K., Zoghbi H.Y. and Orr H.T. (2004) Gene profiling links SCA1 pathophysiology to glutamate signaling in Purkinje cells of transgenic mice. *Human Molecular Genetics* 13, 2535–2543.

Serra H.G., Duvick L., Zu T., Carlson K., Stevens S., Jorgensen N. *et al.* (2006) RORalpha-mediated Purkinje cell development determines disease severity in adult SCA1 mice. *Cell* 127, 697–708.

Servadio A., Koshy B., Armstrong D., Antalffy B., Orr H.T. and Zoghbi H.Y. (1995) Expression analysis of the ataxin-1 protein in tissues from normal and spinocerebellar ataxia type 1 individuals. *Nature Genetics* 10, 94–98.

Shahbazian M.D., Orr H.T. and Zoghbi H.Y. (2001) Reduction of Purkinje cell pathology in SCA1 transgenic mice by p53 deletion. *Neurobiology of Disease* 8, 974–981.

Shakkottai V.G., Chou C.H., Oddo S., Sailer C.A., Knaus H.G., Gutman G.A. *et al.* (2004) Enhanced neuronal excitability in the absence of neurodegeneration induces cerebellar ataxia. *Journal of Clinical Investigation* 113, 582–590.

Sheldon A.L. and Robinson M.B. (2007) The role of glutamate transporters in neurodegenerative diseases and potential opportunities for intervention. *Neurochemistry International* 51, 333–355.

Skinner P.J., Koshy B.T., Cummings C.J., Klement I.A., Helin K., Servadio A. *et al.* (1997) Ataxin-1 with an expanded glutamine tract alters nuclear matrix-associated structures. *Nature* 389, 971–974.

Smith S.J. (1998) Glia help synapses form and function. *Current Biology* 8, R158–R160.

Spacek J. (1985) Relationships between synaptic junctions, puncta adhaerentia and the spine apparatus at neocortical axo-spinous synapses. A serial section study. *Anatomy and Embryology* 173, 129–135.

Tremblay P., Meiner Z., Galou M., Heinrich C., Petromilli C., Lisse T. *et al.* (1998) Doxycycline control of prion protein transgene expression modulates prion disease in mice. *Proceedings of the National Academy of Sciences of the U.S.A.* 95, 12580–12585.

Tyler W.J., Zhang X.L., Hartman K., Winterer J., Muller W., Stanton P.K. *et al.* (2006) BDNF increases release probability and the size of a rapidly recycling vesicle pool within rat hippocampal excitatory synapses. *Journal of Physiology* 574, 787–803.

Unger J.W. (1998) Glial reaction in aging and Alzheimer's disease. *Microscopy Research and Technique* 43, 24–28.

Vandaele S., Nordquist D.T., Feddersen R.M., Tretjakoff I., Peterson A.C. and Orr H.T. (1991) Purkinje cell protein-2 regulatory regions and transgene expression in cerebellar compartments. *Genes and Development* 5, 1136–1148.

Ventura R. and Harris K.M. (1999) Three-dimensional relationships between hippocampal synapses and astrocytes. *Journal of Neuroscience* 19, 6897–6906.

Watanabe M. (2002) Glial processes are glued to synapses via Ca(2+)-permeable glutamate receptors. *Trends in Neurosciences* 25, 5–6.

Watase K., Hashimoto K., Kano M., Yamada K., Watanabe M., Inoue Y. *et al.* (1998) Motor discoordination and increased susceptibility to cerebellar injury in GLAST mutant mice. *European Journal of Neuroscience* 10, 976–988.

Watase K., Weeber E.J., Xu B., Antalffy B., Yuva-Paylor L., Hashimoto K. *et al.* (2002) A long CAG repeat in the mouse Sca1 locus replicates SCA1 features and reveals the impact of protein solubility on selective neurodegeneration. *Neuron* 34, 905–919.

Watkins L.R. and Maier S.F. (2003) Glia: a novel drug discovery target for clinical pain. *Nature Reviews Drug Discovery* 2, 973–985.

Zu T., Duvick L.A., Kaytor M.D., Berlinger M.S., Zoghbi H.Y., Clark H.B. *et al.* (2004) Recovery from polyglutamine-induced neuro-degeneration in conditional SCA1 transgenic mice. *Journal of Neuroscience* 24, 8853–8861.

AUTHORS' ADDRESSES

[1] Department of Surgical Sciences
University of Milano-Bicocca
Italy

[2] Laboratorio di Morfologia delle reti Neuronali
Department of Medicina Pubblica Clinica e Preventiva
Seconda Università di Napoli
Italy

[3] These authors contributed equally to this work

Correspondence should be addressed to:
Prof. Michele Papa
Seconda Università di Napoli
Via L. Armanni
5 80138, Napoli
Italy
phone: +39 081 5666011
fax: +39 081 5666011
email: michele.papa@unina2.it